Proceedings of the
Annual Stability Conference
Structural Stability Research Council
Atlanta, Georgia, April 21-24, 2020

Constrained shell finite element method for stability analysis of thin-walled steel members with tapered sections

Sheng Jin[1], Zhanjie Li[2], Shuang Xu[3], Fang Huang[4]

Abstract
This paper presents a recently developed constrained shell finite element method (termed as fFEM in this paper) towards the elastic buckling analysis of thin-walled members and its applicability toward tapered steel sections using a set of numerical examples. Tapered sections have a wide application in steel structures. However, their stability behaviors could be complex and numerical analysis is commonly required to fully capture it (though some simplified analytical solutions may be possible). For thin-walled tapered members, they will also be subjected to the commonly categorized buckling modes: Global (G), Distortional (D), and Local (L) modes. Recently, a fFEM was developed using a force-based approach by defining the GDL modes utilizing the displacement and force characteristics of each mode. The method was then implemented with shell element formulations in ANSYS, which is capable of providing constrained solutions for the elastic buckling analysis of thin-walled members including prismatic and curved sections – either open or closed. Since the mode definitions of the developed fFEM utilize the stiffness of the linear elastic analysis of the member and the restraints are enforced through the degrees of freedom, these definitions and implementation are revisited and their applicability to tapered sections are justified. Then, numerical examples are demonstrated on a set of thin-walled tapered members, including a tapered I-section and a tapered lipped channel section. The complicated buckling behaviors of these members are accordingly investigated through the modal decomposition and identification of fFEM. All these numerical examples demonstrate the potential and applicability of the developed fFEM in analyzing the stability of tapered steel members.

1. Introduction
Due to the high slenderness ratio of each individual element comprising of a thin-walled member, buckling has played a critical role in the behavior of a thin-walled member. The buckling analysis is normally required and the critical buckling stress (or strength) generally serves as a good indicator of the ultimate strength of the thin-walled member. However, this buckling analysis can be quite effortful due to the many possible deformation modes that are generally encountered: local

[1] Assistant Professor, School of Civil Engineering, Chongqing University, <civiljs@cqu.edu.cn>
[2] Assistant Professor, Department of Engineering, SUNY Polytechnic Institute, <<zhanjie.li@sunypoly.edu>
[3] Graduate Research Assistant, School of Civil Engineering, Chongqing University, <929313352@qq.com>
[4] Graduate Research Assistant, School of Civil Engineering, Chongqing University, <461815829@qq.com>

(plate), distortional, and global. As required in the current design specifications, e.g. AISI S100-16 (American Iron and Steel Institute 2016), each buckling mode is treated uniquely due to its significantly different post-buckling behavior. Therefore, the buckling analysis necessitates not only the traditional prediction of the critical stress but also an ability to appropriately identify buckling modes. Several methods, Generalized Beam Theory (GBT), Finite Strip Method (FSM), constrained FSM (cFSM), and constrained Finite Element Method (cFEM), are capable in providing the modal analysis for typical thin-walled members and will be briefly discussed here.

Implemented in the form of an enriched beam element transformed from nodal to modal (G, D, L, etc.) degrees of freedom (DOF), Generalized Beam Theory (Schardt 1989, Davies and Leach 1994, Davies, Leach et al. 1994, Silvestre and Camotim 2002, Silvestre and Camotim 2002) can separate the different buckling modes through the inclusion of the cross sectional deformations. On the other hand, relaying on the fact that the critical buckling lengths of L, G, and D differ from each other significantly, the Finite Strip Method (Cheung 1968, Li and Schafer 2010), based on finite strip elements thus attaching the critical load directly to the buckling length, gains its capability of identifying the buckling modes. Enforced by the mechanic criteria of the mode classes, cFSM (Ádány and Schafer 2006, Li, Abreu et al. 2014) is developed to enable the similar modal analysis capability like GBT. However, currently, GBT and FSM (and cFSM) can only be used in the analysis of uniform cross section members but not tapered members. Meanwhile, Finite Element Method such as ANSYS can simulate tapered members well with shell elements, but the general shell FEM is not capable of buckling modal classification. Hence, researchers introduced the GBT mode definitions into shell FEM, thus developed constrained FEM with the capability of buckling modal analysis similar to cFSM (Casafont, Marimon et al. 2009, Nedelcu and Cucu 2014, Ádány 2018, Ádány, Visy et al. 2018). Compared to commonly used shell FE, such as the SHELL181 element in ANSYS, GBT considers fewer DOFs for a node. Furthermore, the null membrane shear strain assumption and the linear warping (along cross section mid-lines) assumption in GBT for the L, G, and D modes may cause complex reactions in a shell FE. Therefore, sometimes significant differences might be found between the buckling modal results of GBT and the GBT-based cFEM results (Casafont, Marimon et al. 2011). Moreover, so far only the uniform section members are addressed by cFEM.

Based on the general shell formulation, Jin et al. (Jin, Gan et al. 2018, Jin, Li et al. 2019) implemented a new constrained FEM (termed "fFEM" here to differentiate with the other cFEMs) with a new set of L, G, and D mode definitions. This method does not relays on the aforementioned null membrane shear strain or linear warping assumption. Some criteria in defining the basic modes are not even stipulated directly on the shape of deformation. Instead, they are stipulated on the force: the relationship between the deformation of the member, $\boldsymbol{\Delta}$, and the corresponding elastic load $\boldsymbol{P}$, through the elastic stiffness matrix of the member $\boldsymbol{K}_e$:

$$\boldsymbol{P} = \boldsymbol{K}_e \cdot \boldsymbol{\Delta}, \tag{1}$$

means in defining a deformation mode, other than the conventional way of specifying the $\boldsymbol{\Delta}$, an alternative way by specifying the corresponding elastic load $\boldsymbol{P}$ is also feasible. The numerical examples in (Jin, Gan et al. 2018, Jin, Li et al. 2019) demonstrated that although extra nodal DOFs and extra constitutive relationships compared to GBT were considered in the proposed fFEM because of the shell FE it based, the buckling modal classification results are consistent with those of GBT and cFSM. It should be noted also that so far only uniform section members were addressed. However, the implementation of the proposed fFEM does not require the cross section of the member to be uniform, as doesn't the general shell FEM. Therefore the applicability of the method to tapered members is possible and will be discussed and explored in this study.

2. Essentials of fFEM

2.1 Classification of the nodal DOFs

Six DOFs are usually considered for each node of a shell FE: three translation DOFs and three rotation DOFs. In fFEM, all DOFs of a member (note, they are all node related) are categorized into two assemblages: transverse tangential translational DOFs *u*, and the other DOFs *v*.

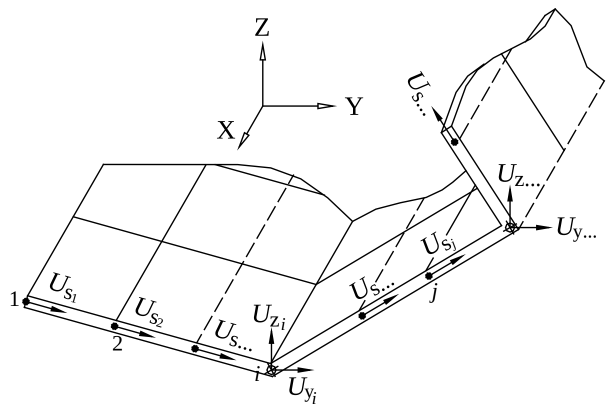

Figure 1: Transverse tangential translational DOFs

All the transverse tangential translational DOFs, *u*-DOFs, in a cross section are pictured in Fig. 1. They are parallel to the mid-lines of the plates with the only exception of the nodes located on the intersection lines between the plates. For an intersection node, the two transverse translation DOFs are both categorized as *u*-DOF, this is because an arbitrary transverse translation of such a node shall produce a translation along the middle line of at least one adjacent element. As a result, considering that there are k nodes in a cross section, and there are p intersection nodes in them, then for this cross section, the number of *u*-DOF is $k+p$, and the number of *v*-DOF is $5k-p$. According to this categorization of the DOFs, the stiffness Eq. (1) can be rewritten as:

$$\begin{Bmatrix} \boldsymbol{Q} \\ \hdashline \boldsymbol{F} \end{Bmatrix} = \begin{bmatrix} \boldsymbol{K}_{\mathrm{Q}} \\ \hdashline \boldsymbol{K}_{\mathrm{F}} \end{bmatrix} \cdot \begin{Bmatrix} \boldsymbol{u} \\ \boldsymbol{v} \end{Bmatrix}, \tag{2}$$

where the vector $\boldsymbol{u}$ contains all the nodal transvers tangential translational DOFs on all cross sections of the member, and $\boldsymbol{v}$ contains all the other nodal DOFs (nu and nv, respectively, referring to the numbers of these two sorts DOFs, i.e. the dimensions of the vectors $\boldsymbol{u}$ and $\boldsymbol{v}$). $\boldsymbol{Q}$ and $\boldsymbol{F}$ are the load vectors corresponding to $\boldsymbol{u}$ and $\boldsymbol{v}$, respectively, and then $\boldsymbol{K}_{\mathrm{Q}}$ and $\boldsymbol{K}_{\mathrm{F}}$ are, respectively, submatrices of $\boldsymbol{K}_{\mathrm{e}}$ consists of the rows corresponding to $\boldsymbol{Q}$ and $\boldsymbol{F}$.

Currently, the deformation and buckling modes of thin-walled members are categorized as L, G, and D modes in fFEM. Two other modes, Shear and Transverse extension modes, can be found in GBT and cFSM. In fFEM, a separated shear mode is not needed. This is because in the fFEM definitions of L, G, and D, the null requirement of the membrane shear strain is not used, thus the shear effects are decomposed and incorporated in the L, G, and D modes by means of force-based criteria. Additionally, considering that the effects of transverse extensions have a relatively small influence on the buckling, this mode isn't separated from the defined basic modes in this paper for the simplicity.

2.2 Modal definitions

fFEM defines the L, G, and D modes through four criteria:

Criterion #1: For L deformation mode, all the transverse tangential displacements $\boldsymbol{u}$ are 0.

Criterion #2: For G and D deformation modes, all the external applied forces are null, with the only exception of the transverse tangential forces $\boldsymbol{Q}$.

Criterion #3: For G mode, the "rigid-body" assumption is applied for the transverse tangential displacements $\boldsymbol{u}$.

Criterion #4: For D mode, all the resultant forces and moments of the applied loads on each cross section are null.

The L mode is defined by Criterion #1. In conventional theories like GBT, the Local deformation mode is characterized by (i) the absence of in-plane nodal displacements, and (ii) no longitudinal displacements (Silvestre and Camotim 2002). The Criterion #1 of fFEM satisfies the traditional condition (i), but allows arbitrary longitudinal nodal translations. Such a choice is made because in some cases the longitudinal translations could be quite an important part of the L mode (Silvestre 2007, Gonçalves and Camotim 2016).

It has to be mentioned that there also exist significant longitudinal translations of the cross sections in G and D modes, while their differences to the L mode, or their orthogonality to L, are still guaranteed owing to Criterion #2, which specifies a loading characteristic of the G and D modes: the external loads are only permitted to act along the *u*-DOFs.

The Criterion #1 means

$$\boldsymbol{u}^{\mathrm{L}} = \mathbf{0}\,, \tag{3}$$

while the Criterion #2 can be expressed as

$$\boldsymbol{F}^{\mathrm{G}} = \mathbf{0}\,, \tag{4}$$

and

$$\boldsymbol{F}^{\mathrm{D}} = \mathbf{0}\,. \tag{5}$$

Thus the orthogonality of the L deformation mode to the G or D mode can be achieved, because

$$\left\{\boldsymbol{\Delta}^{\mathrm{L}}\right\}^{\mathrm{T}} \cdot \boldsymbol{P}^{\mathrm{G(D)}} = \left\{\boldsymbol{u}^{\mathrm{L}}\right\}^{\mathrm{T}} \cdot \boldsymbol{Q}^{\mathrm{G(D)}} + \left\{\boldsymbol{v}^{\mathrm{L}}\right\}^{\mathrm{T}} \cdot \boldsymbol{F}^{\mathrm{G(D)}} = 0\,. \tag{6}$$

Should be noted that all the orthogonality in fFEM are with respect to the stiffness of the member.

Now for the separation between the G and D modes, the Criterion #2 just describes their common aspects, which is not capable for an explicit separation between them.

The G mode is further specified through Criterion #3. As is well known, the “rigid-body” assumption is exactly one of the traditional hypotheses for the global modes: flexural, torsional, and flexural-torsional. In fFEM, this assumption is not needed to be applied to the DOFs other than $\boldsymbol{u}$, because Criterion #2 (Eq. (4)) has already defined a condition for each v-DOF, and no more conditions are need.

On each cross section ‘e’ along the member length, Criterion #3 is mathematically written as

$$ {}^{e}\boldsymbol{u}^{\mathrm{G}} = \left[\cos({}^{e}\boldsymbol{\alpha}_{\mathrm{u}}), \quad \sin({}^{e}\boldsymbol{\alpha}_{\mathrm{u}}), \quad {}^{e}\boldsymbol{r}_{\mathrm{u}} \right] \cdot {}^{e}\boldsymbol{\zeta} , \tag{7} $$

where, α_{u} is the inclined angle from the Y- axis to each u-DOF in this cross section on the positive X- plane, r_{u} is the radii of each u-displacement from the origin, and ${}^{e}\zeta$ is an arbitrary 3×1 vector.

Finally, for the D mode, Criterion #4 specifies the loading characteristic. For any cross section ‘e’, this results in:

$$ \left\{ {}^{e}\boldsymbol{Q}^{\mathrm{D}} \right\}^{\mathrm{T}} \cdot \left[\cos({}^{e}\boldsymbol{\alpha}_{\mathrm{u}}), \quad \sin({}^{e}\boldsymbol{\alpha}_{\mathrm{u}}), \quad {}^{e}\boldsymbol{r}_{\mathrm{u}} \right] = \left\{ 0 \quad 0 \quad 0 \right\} . \tag{8} $$

This criterion is actually originated from the requirement of the orthogonality between G and D modes, because from Eq. (8), one can obtain

$$ \left\{ \boldsymbol{P}^{\mathrm{D}} \right\}^{\mathrm{T}} \cdot \boldsymbol{\Delta}^{\mathrm{G}} = \sum_{e} \left(\left\{ {}^{e}\boldsymbol{Q}^{\mathrm{D}} \right\}^{\mathrm{T}} \cdot {}^{e}\boldsymbol{u}^{\mathrm{G}} \right) = 0 , \tag{9} $$

which means the D mode is orthogonal to the G mode with respect to the stiffness of the member.

2.3 Buckling mode decomposition and identification

The problem of buckling modal classification of thin-walled members can usually be boiled down to two problems: modal decomposition and identification. Shortly speaking, modal decomposition is to calculate pure buckling, i.e. the buckling constrained to a certain deformation mode (or class), while identification is to determine the participation of a certain mode within a general buckling deformation.

First, for the L mode, let’s just constrain the corresponding DOFs of the FE model according to Eq. (3), then an FEM linear buckling analysis on this model will result in buckling modes with the deformations satisfying Criterion #1. These are the pure L modes through this modal decomposition.

Then, for the D mode, let’s apply the force condition Eq. (8) on all the cross sections along the member length, the resultant transverse forces and resultant torques, a total of 3 per cross section, should be zeros. Assuming that the FE model is longitudinal divided into c-1 segments, which means c cross sections in total, the null resultant conditions write:

$$\boldsymbol{J}^{\mathrm{T}} \cdot \boldsymbol{Q}^{\mathrm{D}} = \mathbf{0}_{3c\times 1}, \tag{10}$$

where, $\boldsymbol{J}$ is a nv × 3c matrix assembled from the matrices [cos($^{e}\boldsymbol{\alpha}_{\mathrm{u}}$), sin($^{e}\boldsymbol{\alpha}_{\mathrm{u}}$) , $^{e}\boldsymbol{r}_{\mathrm{u}}$] in Eq. (8), and e=1, 2, …, c.

Combining the Eq. (10) for $\boldsymbol{Q}^{\mathrm{D}}$ and the null $\boldsymbol{F}^{\mathrm{D}}$ condition, Eq. (5), along with the stiffness equation (2), the relationships within the D deformation, $\boldsymbol{\Delta}^{\mathrm{D}}$, can be obtained, as

$$\boldsymbol{C}^{\mathrm{D}} \cdot \boldsymbol{\Delta}^{\mathrm{D}} = \mathbf{0}, \tag{11}$$

where $\boldsymbol{C}^{\mathrm{D}}$ is a (nv +3c) × (nu+nv) matrix as the following:

$$\boldsymbol{C}^{\mathrm{D}} = \begin{bmatrix} \boldsymbol{J}^{\mathrm{T}} \cdot \boldsymbol{K}_{\mathrm{Q}} \\ \boldsymbol{K}_{\mathrm{F}} \end{bmatrix}. \tag{12}$$

Eq. (11) can then be introduced into the FE model in the form of constraint equations, a linear buckling analysis on that FE model will lead to pure D buckling results.

Finally, for the G mode, combining together all the rigid-body condition - Eq. (7) for all cross sections along the member length will results in

$$\boldsymbol{u}^{\mathrm{G}} = \boldsymbol{J} \cdot \boldsymbol{\zeta}. \tag{13}$$

Thus the constraint condition for G mode displacements can be obtained by combining Eqs. (13) and (4):

$$\boldsymbol{C}^{\mathrm{G}} \cdot \begin{Bmatrix} \boldsymbol{\Delta}^{\mathrm{G}} \\ \hdashline \boldsymbol{\zeta} \end{Bmatrix} = \mathbf{0}, \tag{14}$$

where $\boldsymbol{C}^{\mathrm{G}}$ is a (nu+nv) × (nu+nv+3c) matrix as

$$\boldsymbol{C}^{\mathrm{G}} = \left[\begin{array}{cc:c} \mathbf{I}_{n\mathrm{u}} & \mathbf{0}_{n\mathrm{u}\times n\mathrm{v}} & -\boldsymbol{J} \\ & \boldsymbol{K}_{\mathrm{F}} & \mathbf{0}_{n\mathrm{v}\times 3c} \end{array}\right]. \tag{15}$$

Similar to the modal decomposition of D, introducing Eq. (14) into the FE model and then performing the linear buckling analysis, we get the pure G buckling results.

As for the implementation of modal identification, there is no need to enforce any above constraint matrix in the FE linear buckling analysis. Normal FEM linear buckling analysis is performed at first. After that, the general buckling deformation resulted from the FEM analysis can be divided into three parts: sub-L, sub-G, and sub-D deformations according to their definition Eqs. (3), (11) , and (14). The strain energy portions contained in these sub-deformations can then be used as their modal participations of the original FE linear buckling mode. For more details of the identification process please see (Jin, Li et al. 2019).

3. Numerical example: web tapered member

An axially compressed I-section member with the length L=3657.6mm as discussed in (Salem 2019) is considered. Both flanges are rectangular while the web is tapered, as shown in Fig. 2. The cross section dimensions are listed in Table 1. A closed formulation was derived by Salem (Salem 2019) aiming at the flexural buckling around the major-axis of the cross section resulted in a critical load solution P_{cr} = 18093 kN.

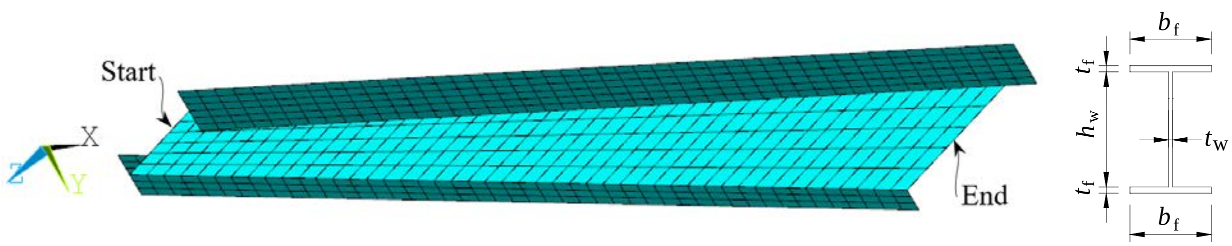

Figure 2: A web tapered I-section member (Salem 2019)

Table 1: Cross section dimensions (Salem 2019)

Location	b_f (mm)	t_f (mm)	h_w (mm)	t_w (mm)
Start	152.4	6.35	304.8	3.175
End	152.4	6.35	609.6	3.175

Modal decomposition of this member is performed here using the aforementioned fFEM. The first step is to build up the shell element model of the member in ANSYS, where SHELL181 (KEYOPT (3) = 2) element is used. The flanges and the web are all discretized into 6 elements transversely, and the longitudinal dimensions of the elements are set to be about 80mm. The elastic modulus E = 200GPa, as in (Salem 2019). In order to compare with the results from that beam element model, the Poisson's ratio is set to be 0. The simple-simple supporting condition is such simulated here: constraining both Y- and Z- translations of all nodes on both ending sections, and constraining the longitudinal translation of an arbitrarily selected node, as explained in (Jin, Gan et al. 2018). The second step is to apply the axial compressions on both ends, which results in the first-ordered stresses in the member. Then, the modal decompositions according to the last section is performed. For this I-section with 3 plates, the distortional mode is commonly not considered. Hence, only the pure L and the pure major-axis flexural (G) buckling are addressed here, and the pure G buckling results will be compared with (Salem 2019). Note the simple-simple supporting condition should be considered in company with the modal constrains (constraint equations). Furthermore, in the calculation of the pure G, all the Y- direction translations of the intersection nodes between the flanges and the web are constrained to prevent the torsion and/or the minor-axis bending of the member.

The first two pure L and pure G buckling modes are listed in Table 2. In this table, the mode sequences and the critical loads are written beside the buckling deformations, signed as terms

"SUB" and "FACT", respectively. From the buckling modes in Table 2, the obtained pure L modes are found to be significantly different from those of uniform cross section members.

Table 2: Pure L and G buckling modes

pure Local buckling mode		pure Global buckling mode	
#1 L	#2 L	#1 G	#2 G
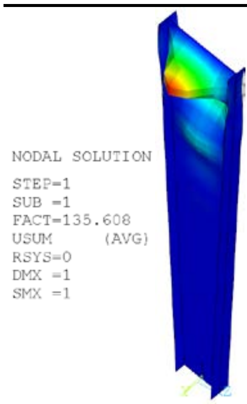	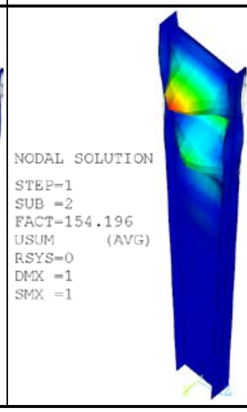	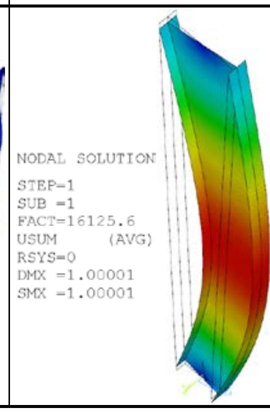	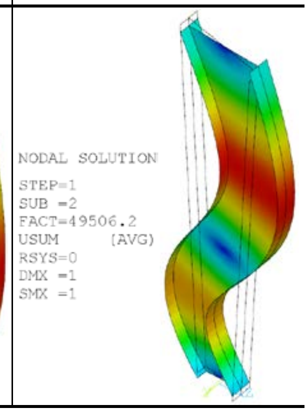

While it is hard to verify these mode definitions similar to those of GBT and cFSM, they do meet our engineering expectations of L and G modes even though the L modes in Table 2 are more localized towards one end. Given the nature of the tapered section, this is expected that a wider end tends to buckle more.

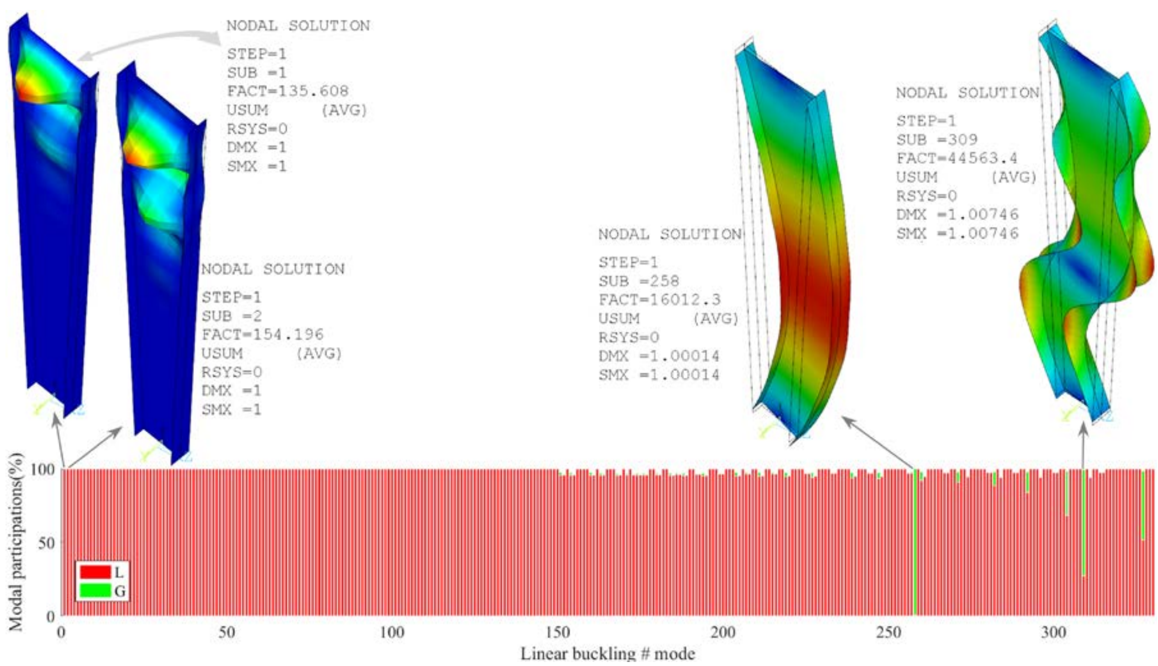

Figure 3: Modal identification of the general FE buckling modes

It has to be admitted that the pure buckling may be different from real buckling, because the pure buckling deformation modes are subjectively stipulated, no matter in GBT, cFSM, or fFEM. Thus it should be interesting to compare these pure buckling results with the general buckling results. For this purpose, a total of 330 general linear buckling modes of the member were calculated. As is well known, among these buckling modes, mostly L dominated modes with different wave-lengths, there exist some individual G dominated ones, while searching through all these buckling deformations to pick them out should be quite boring. Fortunately, the fFEM identification method can calculate the modal participation factors of all these FE buckling deformations automatically and simultaneously, as plotted in Fig. 3. Now it is easy to find out that the first G dominated mode is the #258 mode, the buckling deformation and the critical load are then depicted in Fig. 3, which are quit the same as the #1 pure G results from the decomposition method. Furthermore, the identified second G dominated mode (#309) can be justified by the visual inspection on the corresponding buckling deformation, though it is not that "pure" due to the coupling of the L deformation (which, in turn, can be revealed from the modal participations). Also plotted in Fig. 3 are the #1 and #2 general linear buckling results, which are obviously L dominated, as suggested the modal participation results.

Moreover, it is worth noting that the lowest critical load of the global major-axis flexural buckling obtained in this paper is about 16000kN, which is lower than Salem's result (18093kN) by 12%. This is because, in contrast with the assumptions in (Salem 2019), the effects of the shear deformations on the global buckling have been considered in fFEM. To illustrate this, a further discussion on this web tapered member is to be conducted in the next section.

4. Numerical example: a further discussion on the web tapered member

Some modifications were made to the FE model of the previous example in order to: (i) investigate the effects of the membrane shear strains on this tapered member, and (ii) verify if the proposed method can be applied to other global buckling, e.g. torsional buckling of this member. In doing these, (i) a special shear-panel element, SHELL28, is added for each SHELL181 element using the same nodes. With a sufficiently large shear modulus specified for these SHELL28 elements, the shear deformations are practically excluded in the whole member, as explained in (Ádány and Visy 2012); (ii) all the Y- direction translation constraints on the intersection nodes between the flanges and the web are deleted, so that the torsion and the minor-axis bending are permitted.

The pure G buckling results from the fFEM decomposition with the modified FE model are listed in Table 3, while the identifications on general FE linear buckling modes are shown in Fig. 4. From Table 3 and Fig. 4, following conclusions can be drawn:

(1) The fFEM decomposition and identification method are also applicable for the minor-axis flexural buckling and the torsional buckling of this web tapered member. These buckling modes with different half-wave numbers can be obtained by the decomposition method. Also, they can be identified from general buckling modes by the G participation factors.

(2) The shear deformations do have a significant influence on the major-axis flexural buckling of this tapered member. Without considering this effect, the lowest critical load of the major-axis flexural buckling is very close to that in (Salem 2019).

Table 3 Decomposed pure G modes of modified shear

#1	#2	#4	#10	#21
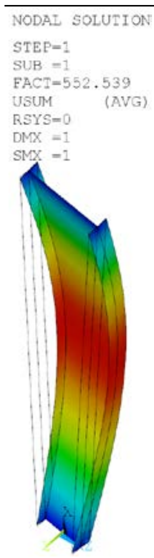	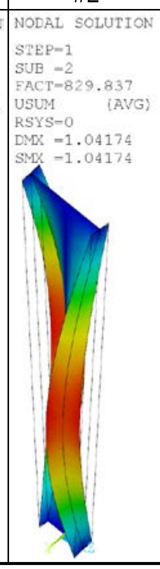	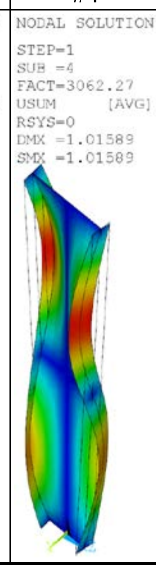	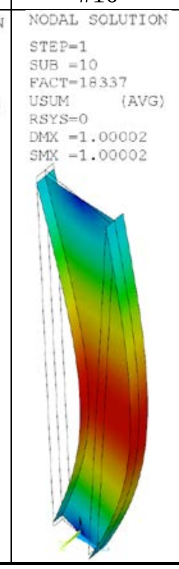	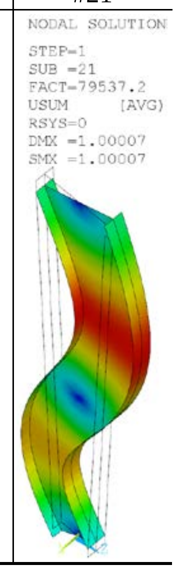

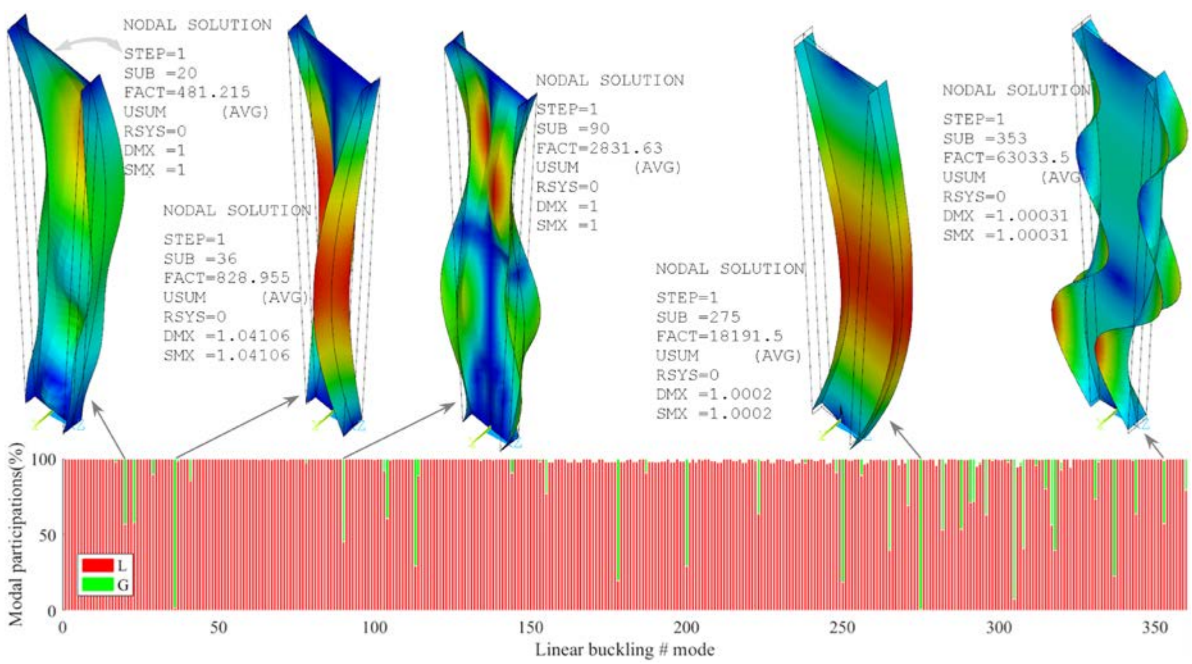

Figure 4: Modal identification on the general FEM linear buckling solutions of modified shear

5. Numerical example: lipped channel

A simply-simply supported and axially compressed tapered lipped channel is considered in this section. This channel has a starting cross section with a web height of 120mm, a flange width of 80mm and a lip length of 20mm, while ends with a section half the dimensions of the starting section. Note all plates have a uniform thickness of 1 mm. The material is assumed to be linear elastic, isotropic, with a Young's modulus of 210 GPa and a Poisson's ratio of 0.3. In terms of the mesh, the cross section is discretized by 4, 6, and 0 intermediate nodes in the flanges, web, and lips, respectively. The longitudinal element dimension is about 15 mm. A 4-node shell element, SHELL63 (KOPT(3)=2), is used in this example, which contains no out-plane shear stiffness, thus more comparable to FSM element than the SHELL181 element previously used.

5.1 Buckling mode decomposition

The 1st pure L, G, and D critical loads of the member with different lengths calculated using fFEM are plotted in Fig. 5. For tapered members, do theses pure mode solutions still hold the representative characteristics of general buckling as in the case of uniform cross section members illustrated in (Jin, Li et al. 2019)? To answer this question, 500 members with different lengths up to 5000mm were analyzed. For each member, all the general buckling modes with critical loads capped at 120 kN are captured and plotted into Fig. 5 as dots. Then, by comparing the pure buckling results to the general buckling results, the following conclusions can be drawn:

(1) These dots, i.e. the 1st, 2nd, etc. critical loads of the general buckling of the member with different lengths, form series critical curves according to different transverse deformation patterns and/or longitudinal wave-numbers. In all these curves, there is a special one, which holds the lowest position when the members is shorter than 2000 mm, and which is well agreed by the pure L solutions from the fFEM decomposition.

(2) There is another curve which is quite close to the pure G solutions, and which is the lowest when the member is longer than 2000 mm.

(3) Many higher curves, i.e. higher buckling modes, show some consistencies to the two lowest curves aforementioned, but there do exist some special parts show different patterns, e.g. those aligned with the pure D solutions.

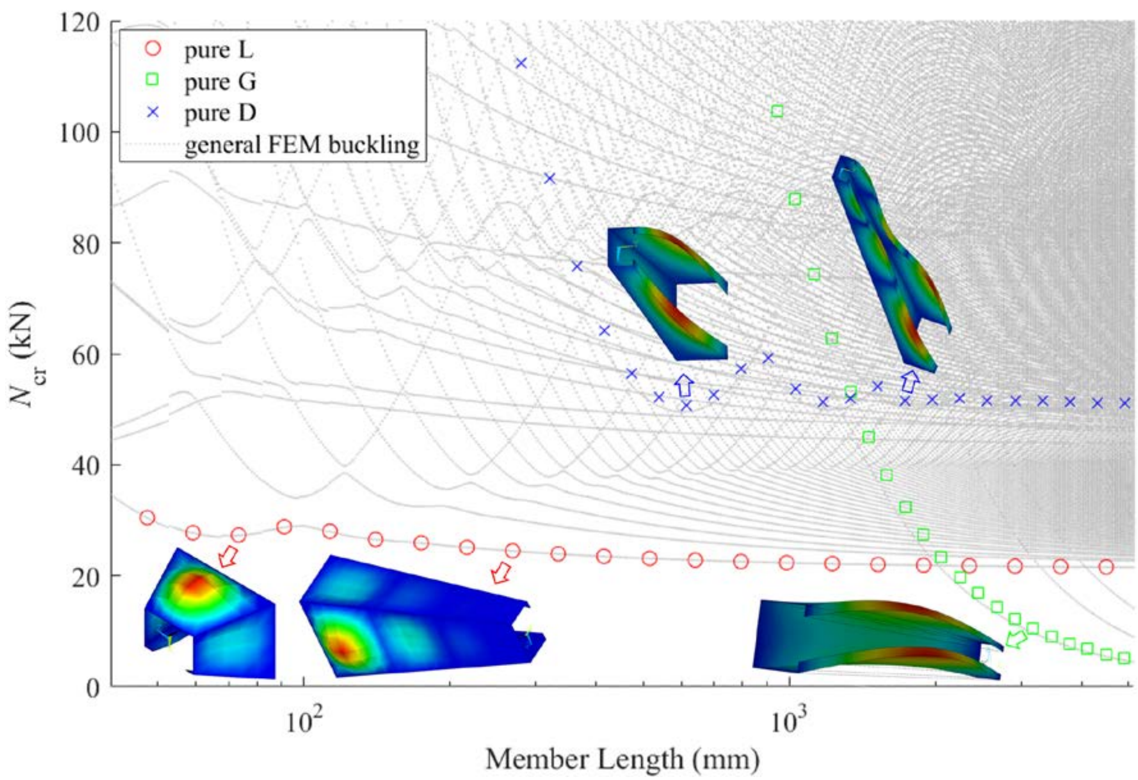

Figure 5: Pure 1st G, D, L vs. general FE buckling

Thus, for this axially compressed tapered channel, the proposed L, G, and D modes do hold some main aspects of its linear buckling. The pure mode buckling deformations depicted in Fig. 5 show well agreements with those well-known modes of uniform section members. However, the tapering of the member do change something, as clearly observed by the mode shapes especially longitudinally patterns.

5.2 Buckling mode identification

As illustrated in Fig. 5, the various transverse deformation patterns and the arbitrary choices of longitudinal half-wave numbers of the buckling deformation lead to a large amount of general buckling results. The pure L, G, and D results help identifying some of general buckling modes but not all. Also the pure buckling results are different from the general buckling results, especially for the higher-ordered buckling modes. Thus, an identification directly on the general buckling results are performed. The fFEM identification method was applied on all these general buckling modes. The resulted L, G, and D participations are then used to render the corresponding dots of the modes in RGB format (Red : Green : Blue = L : G : D participations), as illustrated in Fig. 6.

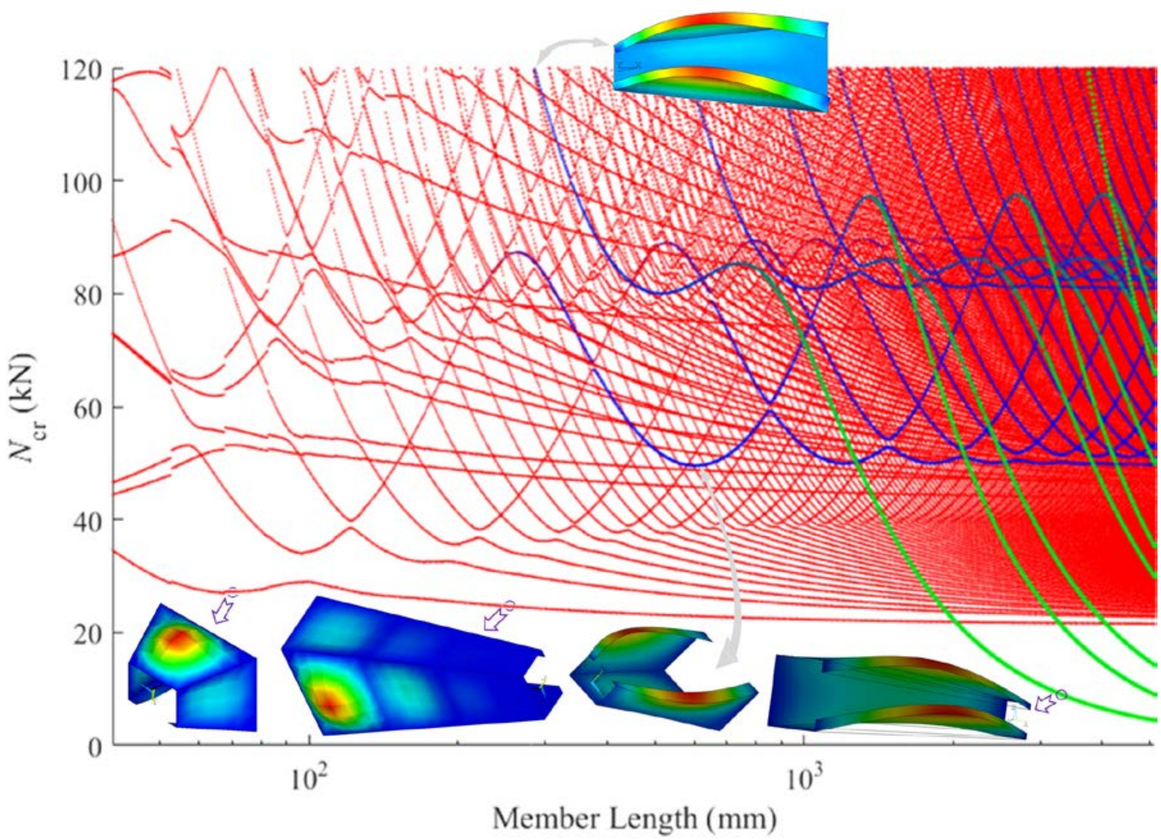

Figure 6: Identification of the general FE buckling modes

The buckling mode identification helps explaining the inherent trends in the general FEM buckling results shown in Figs. 5 and 6. Obviously, the automatically identified D or G dominant modes from the vast majority of the L dominant modes agree with the engineering expectation, as illustrated by the buckling shapes in Fig. 6.

5.3 The effects of the section tapering

In investigating the effects of the section tapering, a member with a uniform cross section, simply-simply supported and axially compressed as well, was analyzed and compared. The uniform cross section considered here was in the average dimensions of previous tapered section, i.e. a web height of 90mm, a flange width of 60mm, a lip length of 15mm, and a thickness of 1mm. Same SHELL63 element and same discretization pattern were used. The pure L, G, and D buckling results of these two sorts of members are compared in Fig. 7. The FSM signature curve of the uniform section member from CUFSM (Schafer 2018) is also plotted. A same cross section discretization is used for the CUFSM model.

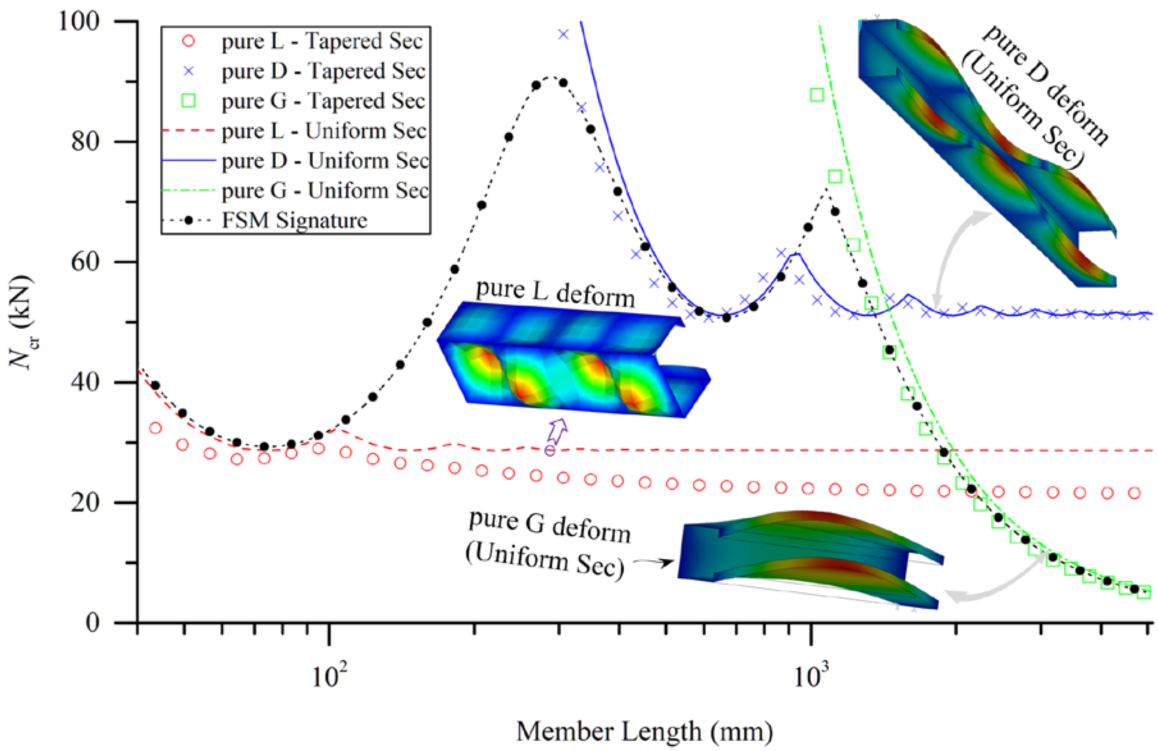

Figure 7: Buckling mode decomposition: tapered section vs. uniform section

From Fig. 7, it can be found for this uniform section member that the pure L, G, and D results agree well with specific parts of the FSM signature curve, which shows the applicability of the fFEM for uniform section members. As far as the effects of the section tapering on the buckling, by comparisons with the uniform section member, they can be concluded as follows:

(1) The local buckling deformation of the tapered member occurs mainly in the region near the bigger end, resulting in a lower critical load compared to the uniform section member. This is because the average cross section of this region is larger than the uniform section. Further, the average cross section of this region gets larger with the increase of the member length, leading to lower critical L loads.

(2) It can be observed that the G and D buckling deformations, in contrast, occur along the whole length of the tapered member, thus the pure G and D critical loads are quite close to those of the uniform section member, though, in terms of the G critical load and the D critical wave-length, small discrepancies can still be found.

6. Discussions

In this paper, only the loading condition of axially compressed are considered with the supporting condition limited to simple-simple case. Actually, the fFEM, and of course the shell FEM it is based on, can be applicable for more loading and supporting conditions but not investigated in this paper.

In addition, only the open polygon cross section is considered here. A study on curved cross sections should be interesting as well as closed cross sections, noting the contradiction of the traditional theories in handling the torsion, which is normally considered as a global mode but governed by the membrane shear effects. The new treatment on the membrane shear effects in the fFEM definitions should be of help in resolving it.

7. Conclusions

The development of a new constrained shell Finite Element Method (fFEM) paves a way for a broader application of the shell FEM by enabling the modal decomposition and identification in elastic buckling analysis of thin-walled tapered members. Since the mode definitions of the fFEM utilize the stiffness of the linear elastic analysis of the member and the restraints are enforced through the degrees of freedom, these definitions and implementation are revisited. Numerical examples using a tapered I-section and a tapered lipped channel section under compression demonstrate the applicability of the method to tapered members. In particular, the pure modes from modal decomposition meet our engineering expectations and their critical loads agree well with the general FEM buckling solutions for the corresponding modes. The impact of the tapering on the lipped channel is investigated. The tapering has a large impact on the critical loads of local buckling especially long members and small impacts on the global and distortional buckling. All these numerical examples demonstrate that the fFEM is able to capture the tapering effects on the buckling behaviors and can potentially aid the analysis of tapered steel members although more studies are needed.

Acknowledgements

The support of this work by the National Program on Key Research and Development Project (No. 2017YFC0703805) and the Natural Science Foundation Project of CQ CSTC (No. cstc2017jcyjAX0341) is gratefully acknowledged.

References

Ádány, S. (2018). "Constrained shell Finite Element Method for thin-walled members, Part 1: constraints for a single band of finite elements." Thin-Walled Structures 128: 43-55.

Ádány, S. and B. W. Schafer (2006). "Buckling mode decomposition of single-branched open cross-section members via finite strip method: Derivation." Thin-Walled Structures 44(5): 563-584.

Ádány, S. and D. Visy (2012). "Global buckling of thin-walled simply supported columns: Numerical studies." Thin-Walled Structures 54: 82-93.

Ádány, S., D. Visy and R. Nagy (2018). "Constrained shell Finite Element Method, Part 2: application to linear buckling analysis of thin-walled members." Thin-Walled Structures 128: 56-70.

American Iron and Steel Institute (2016). North American Specification for the Design of Cold-Formed Steel Structural Members (2016 Edition). Washington (DC).

Casafont, M., F. Marimon, M. Pastor and M. Ferrer (2011). "Linear buckling analysis of thin-walled members combining the Generalised Beam Theory and the Finite Element Method." Computers & Structures 89(21–22): 1982-2000.

Casafont, M., F. Marimon and M. M. Pastor (2009). "Calculation of pure distortional elastic buckling loads of members subjected to compression via the finite element method." Thin-Walled Structures 47(6–7): 701-729.

Cheung, Y. K. (1968). "The Finite Strip Method in the Analys of Elastic Plates with Two Opposite Simply Supported Ends." Proceedings of the Institution of Civil Engineers 40(1): 1-7.

Davies, J. M. and P. Leach (1994). "First-order generalised beam theory." Journal of Constructional Steel Research 31(2-3): 187-220.

Davies, J. M., P. Leach and D. Heinz (1994). "Second-order generalised beam theory." Journal of Constructional Steel Research 31(2-3): 221-241.

Gonçalves, R. and D. Camotim (2016). "GBT deformation modes for curved thin-walled cross-sections based on a mid-line polygonal approximation." Thin-Walled Structures 103: 231-243.

Jin, S., D. Gan, H. Chen, R. Cheng and X. Zhou (2018). "A force-based method for identifying the deformation modes of thin-walled members." Thin-Walled Structures 129: 473-487.

Jin, S., Z. Li, F. Huang, D. Gan, R. Cheng and G. Deng (2019). "Constrained shell finite element method for elastic buckling analysis of thin-walled members." Thin-Walled Structures 145: 106409.

Li, Z. and B. W. Schafer (2010). "Application of the finite strip method in cold-formed steel member design." Journal of Constructional Steel Research 66(8-9): 971-980.

Li, Z. J., J. C. B. Abreu, J. Z. Leng, S. Adany and B. W. Schafer (2014). "Review: Constrained finite strip method developments and applications in cold-formed steel design." Thin-Walled Structures 81: 2-18.

Nedelcu, M. and H. L. Cucu (2014). "Buckling modes identification from FEA of thin-walled members using only GBT cross-sectional deformation modes." Thin-Walled Structures 81: 150-158.

Salem, E. S. (2019). Stiffness matrix for buckling analysis of tapered steel members. SSRC 2019 Annual Stability Conference, St. Louis, Missouri.

Schafer, B. W. (2018). CUFSM 5.01—Elastic Buckling Analysis of Thin-walled Members by the Finite Strip Method and Constrained Finite Strip Method for General End Boundary Conditions. Department of Civil Engineering, Johns Hopkins University. <http://www.ce.jhu.edu/bschafer/cufsm/>.

Schardt, R. (1989). Verallgemeinerte Technische Biegetheorie [Generalised Beam Theory]. Berlin, Springer Verlag.

Silvestre, N. (2007). "Generalised beam theory to analyse the buckling behaviour of circular cylindrical shells and tubes." Thin-Walled Structures 45(2): 185-198.

Silvestre, N. and D. Camotim (2002). "First-order generalised beam theory for arbitrary orthotropic materials." Thin-Walled Structures 40(9): 755-789.

Silvestre, N. and D. Camotim (2002). "Second-order generalised beam theory for arbitrary orthotropic materials." Thin-Walled Structures 40(9): 791-820.